

Kondo Breakdown via Fractionalization in a Frustrated Kondo Lattice Model

Johannes S. Hofmann,^{1,*} Fakher F. Assaad,^{1,†} and Tarun Grover^{2,‡}

¹*Institut für Theoretische Physik und Astrophysik, Universität Würzburg, Am Hubland, D-97074 Würzburg, Germany*

²*Department of Physics, University of California at San Diego, La Jolla, CA 92093, USA*

We consider Dirac electrons on the honeycomb lattice Kondo coupled to spin-1/2 degrees of freedom on the kagome lattice. The interactions between the spins are chosen along the lines of the Balents-Fisher-Girvin model that is known to host a \mathbb{Z}_2 spin liquid and a ferromagnetic phase. The model is amenable to sign free auxiliary field quantum Monte Carlo simulations. While in the ferromagnetic phase the Dirac electrons acquire a gap, they remain massless in the \mathbb{Z}_2 spin liquid phase due to the breakdown of Kondo screening. Since our model has an odd number of spins per unit cell, this phase is a non-Fermi liquid that violates the conventional Luttinger theorem which relates the Fermi surface volume to the particle density in a Fermi liquid. This non-Fermi liquid is a specific realization of the so called fractionalized Fermi liquid proposed in the context of heavy fermions. We probe the Kondo breakdown in this non-Fermi liquid phase via conventional observables such as the spectral function, and also by studying the mutual information between the electrons and the spins.

Introduction: Electron-electron interactions can localize charge carriers and generate insulating states with local moments [1]. What happens when these local moments (f-spins) are Kondo coupled with magnitude J_K to extended Bloch conduction (c-) electrons? For a single local moment, the answer is known: the Kondo coupling is relevant and the f-electron is screened by the conduction electrons [2, 3]. For a lattice of f-electrons i.e. Kondo lattice systems, the problem is much harder, and the answer is not known in general. However, in the absence of any magnetic ordering, Lieb-Shultz-Mattis-Hastings-Oshikawa theorem [4–6] puts strong constraints on the possible outcomes. Specifically, in addition to a heavy Fermi liquid phase where the Fermi surface is ‘large’ since it includes the local moments, there exists a distinct possibility where f-spins decouple from the conduction electrons at low-energies and enter a spin-liquid phase [7, 8]. In such a ‘fractionalized Fermi liquid’ phase (henceforth denoted as ‘FL* phase’ following Refs.[7, 8]), the conduction electron Fermi surface is ‘small’ in that it does not include local moments, and therefore the conventional Luttinger theorem [9] is violated.

From an experimental standpoint, a possible breakdown of Kondo screening is relevant to some of the most challenging issues in heavy fermion materials [7, 10, 11]. There are at least two conceptually different scenarios where a breakdown of Kondo screening might play a role: in materials such as YbRh_2Si_2 [12] and $\text{CeCu}_{6-x}\text{Au}_x$ [13], one observes signatures that indicate that Kondo screening might abruptly change across the transition from a heavy Fermi liquid phase to a magnetically ordered phase. For example, in YbRh_2Si_2 , one observes a jump in the Hall coefficient across the phase transition while in $\text{CeCu}_{6-x}\text{Au}_x$, one finds that the single ion Kondo energy scale T_K exhibits an abrupt change close the quantum critical point. A different scenario, which is perhaps more closely related to this paper is the transition from

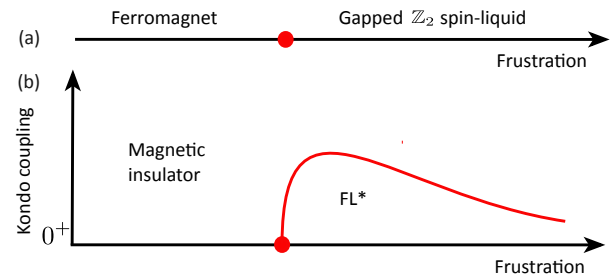


FIG. 1. (color online) (a) Schematic phase diagram of the BFG model in the absence of Kondo coupling. (b) Schematic phase diagram of the BFG model in the presence of Kondo coupling.

a heavy Fermi liquid to a *non-magnetic* phase across which Kondo screening breaks down. Signatures of such a phase were seen in Co and Ir doped YbRh_2Si_2 [14]. Following Refs. [4, 7, 8] and as discussed above briefly, in the absence of any other symmetry breaking (e.g. lattice translation) such a non-magnetic phase is inconsistent with a Fermi liquid ground state if the Kondo screening is not operative and the unit cell contains an odd number of spin-1/2 spins. The local moments in such a phase are then forced to either have a gapless spectrum or topological order [5]. We also note that as discussed in Ref. [15], the Kondo breakdown is also closely related to the concept of ‘orbital selective Mott transition’. In addition, there are several other heavy fermionic materials such as CePdAl [16–19], $\kappa\text{-(ET)}_4\text{Hg}_{2.89}\text{Br}_8$ [20], YbAgGe [21], YbAl_3C_3 [22] and $\text{Yb}_2\text{Pt}_2\text{Pb}$ [23] whose phenomenology seems to be poorly understood, and where microscopic considerations suggest that the geometric frustration between local moments plays an important role.

In this paper we will introduce a generalized Kondo lattice model which hosts the aforementioned Kondo breakdown transition between a conventional phase with electron like quasiparticles, and an FL* phase with \mathbb{Z}_2 topological order. From a technical standpoint, the most salient feature of our model is that it does not suffer from fermion sign problem even in the presence of the Kondo coupling [24]. Our model

* johannes.hofmann@physik.uni-wuerzburg.de

† assaad@physik.uni-wuerzburg.de

‡ tagrover@ucsd.edu

is realized by Kondo coupling a variant of the Balents-Fisher-Girvin (BFG) model [25–27], first introduced in Ref. [28], to conduction electrons. The BFG model supports a transition from a ferromagnetic phase to a gapped \mathbb{Z}_2 spin-liquid (Fig. 1(a)). When this model is weakly coupled to conduction electrons, the spin-liquid gives way to an FL* phase where the conduction electrons form a Dirac semi-metal, while the local moments continue to form a \mathbb{Z}_2 spin-liquid (Fig.1(b)). Since our unit cell contains two c-electrons and three f-spins, this result stands at odds with the Luttinger sum rule. As the Kondo coupling is increased beyond a threshold, one loses the topological order of local moments, and enters a conventional phase with electron like quasiparticles. We will characterize the Kondo breakdown by studying the spectral function of the conduction electrons, and also via the mutual information between the conduction electrons and local moments.

Model and limiting cases: We investigate the following generalized Kondo lattice model (KLM) described by $\hat{H} = \hat{H}_c + \hat{H}_S + \hat{H}_K$ with:

$$\hat{H}_c = -t \sum_{\langle \mathbf{x}, \mathbf{y} \rangle, \sigma} \hat{c}_{\mathbf{x}, \sigma}^\dagger \hat{c}_{\mathbf{y}, \sigma} + h.c. \quad (1)$$

$$\hat{H}_S = -J^\perp \sum_{\langle \mathbf{i}, \mathbf{j} \rangle} \left(\hat{S}_i^{f,+} \hat{S}_j^{f,-} + h.c. \right) + J^z \sum_{\square} \left(\hat{S}_\square^{f,z} \right)^2$$

$$\hat{H}_K = J_K \sum_{\langle \mathbf{x}, \mathbf{i} \rangle} \left[\hat{S}_x^{c,z} \hat{S}_i^{f,z} - (-1)^{\mathbf{x}} \left(\hat{S}_x^{c,+} \hat{S}_i^{f,-} + h.c. \right) \right].$$

Here, $\hat{c}_{\mathbf{x}, \sigma}^\dagger$ creates a conduction electron in a Wannier state centered at \mathbf{x} with a z-component of spin σ , $\mathbf{S}_x^c = \frac{1}{2} \sum_{s, s'} \hat{c}_{x, s}^\dagger \boldsymbol{\sigma}_{s, s'} \hat{c}_{x, s'}$ is the spin operator and $\langle \mathbf{x}, \mathbf{y} \rangle$ are the nearest neighbors of a honeycomb lattice. \mathbf{S}_i^f is a spin-1/2 degree of freedom located on the kagome lattice corresponding to the median of the honeycomb lattice (see Fig.2). The Hamiltonian \hat{H}_S is a variant of the BFG model (Ref. [25, 28]) with nearest neighbor, $\langle \mathbf{i}, \mathbf{j} \rangle$, spin flip amplitude J^\perp and interaction, J^z that minimizes the total z-component of spin on a hexagon: $\hat{S}_\square^{f,z} = \sum_{\mathbf{i} \in \square} \hat{S}_i^{f,z}$. The conduction electrons and the local moments are Kondo coupled, according to \hat{H}_K , along nearest neighbor bonds $\langle \mathbf{x}, \mathbf{i} \rangle$ between the kagome and Honeycomb lattices (Fig. 2). The factor $(-1)^{\mathbf{x}}$ that takes the value 1 (-1) on the A (B) sublattice of the Honeycomb lattice is necessary to avoid the negative sign problem. In particular it cannot be gauged away since the kagome lattice is not bipartite. Referring back to Fig.1, J^z plays the role of frustration, and J_K is the Kondo coupling.

Let us consider various limiting cases of the Hamiltonian \hat{H} . When $J^\perp \gg J^z, J_K$, the local moments order in an XY-ferromagnetic ground state. Taking into account the $(-1)^{\mathbf{x}}$ factor in the Kondo coupling, we see that this terms induces an anti-ferromagnetic in-plane mass term for the conduction electrons. Hence, in this limit one obtains a magnetically ordered insulating phase.

Next, consider $J_K \gg J^\perp \gtrsim J^z, t$. First, let us set all couplings except J_K to zero. Performing the unitary transformation $\hat{c}_{\mathbf{x}, \downarrow} \rightarrow -(-1)^{\mathbf{x}} \hat{c}_{\mathbf{x}, \downarrow}$ maps the Kondo interaction to an

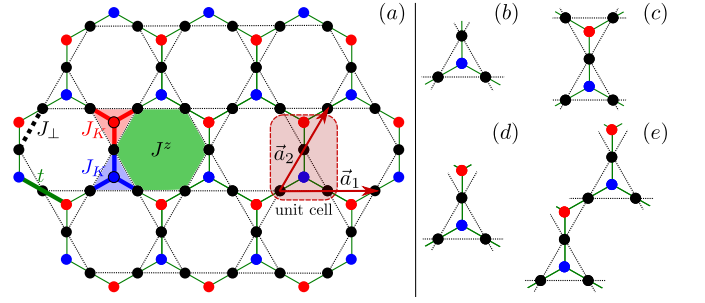


FIG. 2. (color online) *Left:* The model - The conduction (c) electrons hop, with matrix element t , between nearest neighbor sites of the honeycomb lattice denoted by the red and blue circles. The kagome lattice (black) supports impurity spins described by the Balents-Fisher-Girvin model with nearest neighbor spin-flip J^\perp and interactions on hexagons of strength J^z (green). The two systems are Kondo-coupled with strength J_K for each bond in the elemental triangles (thick red and blue bonds). For details see Eq. (1). *Right:* Various patches Γ used to extract the Renyi mutual information. Subsets (b) and (c) belong to the triangle sequence, (d) and (e) are built out of unit cells.

anti-ferromagnetic Heisenberg coupling between the conduction electrons and the local moments. This interaction is not frustrated, and the ground state is AFM ordered with opposite polarizations on the kagome sites and the Honeycomb lattice. Undoing the above transformation, the in-plane magnetization of the conduction electrons will be parallel for one honeycomb sublattice and anti-parallel for the other, relative to the local moments. Next, turning on a small J^\perp, J^z with $J^\perp \gtrsim J^z$, the local moments will preferably order in the XY plane. Comparing to the limit $J^\perp \gg J^z, J_K$, one finds that the in-plane symmetry breaking pattern is identical and in the absence of any out-of-plane component, this phase is expected to be adiabatically connected to the aforementioned magnetically ordered insulating phase in the $J^\perp \gg J^z, J_K$ limit. Note that an out-of-plane component will spontaneously break the symmetry $\hat{S}_i^{f,z} \rightarrow -\hat{S}_i^{f,z}, \hat{S}_i^{f,x} \rightarrow \hat{S}_i^{f,x}, \hat{S}_i^{f,y} \rightarrow \hat{S}_i^{f,y}$ (see the supplemental material for a detailed discussion of the symmetries). Due to symmetry breaking and associated stiffness, this phase is stable also to switching on a small hopping t .

Most interesting is the limit $J^z \gg J^\perp \gg J_K$. When only J^z and t are non-zero, the conduction electrons form a Dirac semimetal while the local moments can be described as a classical system with a ground state degeneracy that scales exponentially with the system size [25]. Allowing a small $J^\perp/J^z \ll 1$ lifts this macroscopic degeneracy and leads to a \mathbb{Z}_2 topologically ordered spin liquid of the local moments [25]. Remarkably, as discussed in Refs. [7, 8], introducing a small Kondo coupling J_K leaves the state unchanged because perturbatively the Kondo coupling is irrelevant at the renormalization group fixed point where conduction electrons form a Dirac semimetal while the local moments are in a gapped \mathbb{Z}_2 topologically ordered state. Therefore, at low energies, the local moments decouple from the conduction electrons and one obtains a non-Fermi liquid FL* phase with a ‘small’ Fermi

surface which was introduced in Refs.[7, 8]. Physically, in this phase the local moments are highly entangled with each other such that the formation of Kondo singlets or the tendency to magnetically order is suppressed.

The phases discussed above, especially the FL* phase, should be contrasted with the conventional heavy Fermi liquid that satisfies the Luttinger sum rule. Since our model has two electrons and three spins per unit cell, the most prominent feature is that this state has a ‘large’ Fermi surface which encloses half of the BZ whereas the Fermi volume of the aforementioned fractionalized FL* phase vanishes. The nature of the Fermi liquid state strongly depends on symmetries. If particle hole-symmetry (PHS) is imposed in the paramagnetic phase, then one would expect a flat-band pinned at the Fermi level, a generically unstable state [29–37]. A hybridization between c - and f -electrons necessarily breaks either PHS - with uniform hybridization - or TRS - when the $(-1)^{\mathbf{x}}$ phase in the Kondo coupling is carried over to the hybridization. The latter requires fine-tuning to remain paramagnetic whereas the former can generate a non-magnetic heavy Fermi liquid. In the range of parameters considered in this paper, we do not find such a phase. A more detailed discussion can be found in the supplemental material.

Method and observables: We simulate the Hamiltonian in Eq. (1) using the auxiliary field quantum Monte Carlo (QMC) method [38–40]. We follow the strategy outlined in Ref. [24] where it was shown that Hamiltonians of the form \hat{H} do not suffer from fermion sign problem when $J^\perp \geq 0$ and the conduction bands are particle-hole symmetric. In this approach local moments are fermionized, $\mathbf{S}_i^f = \frac{1}{2} \sum_{s,s'} \hat{f}_{i,s}^\dagger \boldsymbol{\sigma}_{s,s'} \hat{f}_{i,s'}$, with the constraint $\sum_s \hat{f}_{i,s}^\dagger \hat{f}_{i,s} = 1$. As in simulations of the generic Kondo lattice model [41, 42] this constraint can be imposed very efficiently since it corresponds to a local conservation law. The details of our implementation are summarized in the supplemental material and we have used the ALF package [43] to carry out the simulations. Despite the absence of sign problem, the simulations of this model are challenging. Fermionization leads to a large number of auxiliary fields (33 per unit cell), and the *condition number* on scales corresponding to the ratio of *band width* to the smallest relevant scale (e.g. vison gap in the \mathbb{Z}_2 spin liquid phase) is large. As a consequence, we have used an imaginary time step $\Delta\tau t = 0.01$. The biggest challenge turns out to be large autocorrelation times. We tried to improve this issue by using global moves that mimic vison excitations, as well as by implementing parallel tempering schemes. Nevertheless, these long autocorrelation times remain the limiting factor to access system sizes bigger than those presented here, in particular 3×3 and 6×3 unit cells. For both lattices sizes, and the considered periodic boundary conditions, Dirac points are present. However, only the 6×3 allows to satisfy $\hat{S}_\Omega^{f,z} = 0$ for all hexagons.

We compute spin-spin correlations $S_{AFM} = 1/L \sum_{\mathbf{I}\mathbf{J}} \langle \hat{S}_\mathbf{I}^x \hat{S}_\mathbf{J}^x + \hat{S}_\mathbf{I}^y \hat{S}_\mathbf{J}^y \rangle$ where the net spin per unit cell \mathbf{I} , $\hat{\mathbf{S}}_\mathbf{I} = \sum_{i \in \mathbf{I}} \hat{\mathbf{S}}_i^f + \sum_{\mathbf{x} \in \mathbf{I}} (-1)^{\mathbf{x}} \hat{\mathbf{S}}_{\mathbf{x}}^c$, captures the

mentioned ferromagnetic-antiferromagnetic order of the f -spins and conduction electrons. The spectral function of the conduction electrons $A_c(\mathbf{k}, \omega) = -\frac{1}{\pi} \text{Im} G_c^{\text{ret}}(\mathbf{k}, \omega)$ can be extracted from the imaginary time resolved Greens function $G_c(\mathbf{k}, \tau) = \sum_{\alpha,\sigma} \langle \hat{c}_{\mathbf{k},\alpha,\sigma}^\dagger(\tau) \hat{c}_{\mathbf{k},\alpha,\sigma}(0) \rangle$ using the MaxEnt method [44, 45]. Here α is the orbital index. The auxiliary field QMC method also allows to study the entanglement properties of fermionic models [46–51]. In particular, as shown in Refs. [47, 48], the second Renyi entropy S_2 can be computed from the knowledge of Greens-functions G_A , restricted to subsystem A for two independent Monte Carlo samples. An alternative approach exploits the replica trick, e.g. for fermionic [52–55], bosonic [28], and spin systems [56, 57]. For a given subsystem of conduction electrons Γ_c and of spins Γ_f , the Renyi mutual information between Γ_c and Γ_f is $I_2(\Gamma_c, \Gamma_f) \equiv S_2(\Gamma_c \cup \Gamma_f) - S_2(\Gamma_c) - S_2(\Gamma_f)$. We use the two sequences for Γ as shown in Fig. 2(b), (c) and, Fig. 2(d),(e). In the calculation of the Renyi mutual information we restore the C_3 lattice symmetry by averaging over rotationally equivalent Γ s.

Results: From here on, we fix $J^\perp = t$ and use $t = 1$ as the unit of energy. The BFG model shows a transition from the ferromagnetic state to the \mathbb{Z}_2 spin liquid at $J_c^z \simeq 7.07$ [28]. Alongside with spin excitations, the \mathbb{Z}_2 spin liquid hosts vison excitations. Recent simulations of the dynamics of the BFG model [58] estimate the spin and vison gaps at $J^z = 8.3$ to $\Delta_s \simeq 7.12$ and $\Delta_v \simeq 0.2$. We expect that the vison gap remains non-zero at the transition and that the spin gap scales as $(J^z - J_c^z)^\nu$ with dynamical critical exponent $z = 1$ and $\nu \simeq 0.67$, which correspond to the exponents of the 3D XY* model [26, 59, 60].

Fig. 3 shows a scan at $J^z = 7.5$ as a function of J_K . We have set the temperature to $\beta = 12$. From the above discussion, this choice of temperature places us well below the spin gap and allows us to resolve the vison gap. As apparent in Fig. 3(c), the single particle spectral function at the Dirac point remains gapless. As a function of J_K it loses spectral weight and a full gap opens slightly before $J_K = 1.5$. At this energy scale the spin-spin correlations S_{AFM} show a marked upturn (see Fig. 3(a)). In the presence of long ranged magnetic order S_{AFM} scales as the volume of the system. Comparison between the 3×3 and 3×6 lattices shows that S_{AFM} grows as a function of system size beyond $J_K = 1.5$.

Small values of J_K are associated with small energy scales which may be difficult to resolve on our finite sized systems at finite temperatures. To confirm above result, we present a scan at fixed $J_K = 1$ and vary J^z in Fig. 4. Upon analysis of Figs. 4(a) and 4(c) one concludes that the magnetic order and the single particle gap track each other. In particular the single particle gap closes in the \mathbb{Z}_2 spin liquid phase.

Signatures of the \mathbb{Z}_2 spin liquid phase can be picked up in the spectrum of the conduction electrons. In Fig. 3(d) and Fig. 4(d) we plot the single particle spectral function at the Γ point. One notices that in the FL* phase, spectral weight at low energies is apparent. We associate this feature with the vison excitations of the \mathbb{Z}_2 spin liquid.

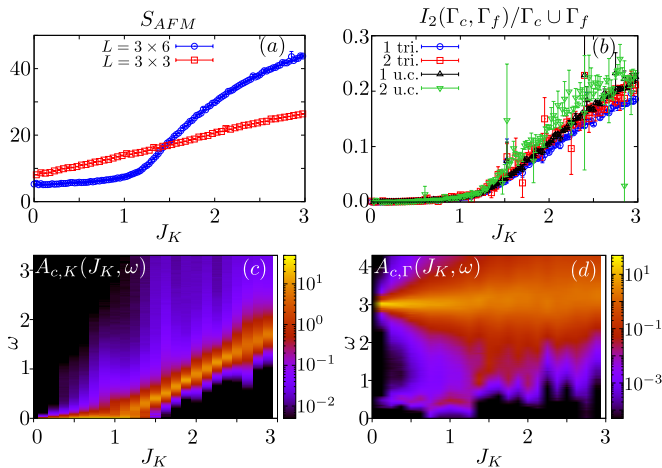


FIG. 3. (color online) We consider lattices $L = 3 \times 3$ and $L = 3 \times 6$ unit cells at an inverse temperature $\beta = 12$ and at $J^z = 7.5$ (a) Spin-spin correlations S_{AFM} (See text), (b) Renyi mutual informations $I_2(\Gamma_c, \Gamma_f)$ per site of the patch $\Gamma_c \cup \Gamma_f$ for $L = 3 \times 6$. Here we consider the patches listed in Fig. 2(b)-(e). (c) Conduction electron spectral function at the Dirac point \mathbf{K} for the 3×6 lattice. (d) Same as (c), but at the Γ -point. The imaginary time data from which panels (c) and (d) stem are presented in the supplemental material.

It is interesting to consider other measures for Kondo screening. The Renyi mutual information I_2 between the c-electrons and the f-spins introduced above provides one such measure. It is important to note that this quantity is both IR and UV sensitive since we are considering mutual information between two Hilbert spaces that overlap in real space. Despite the decoupling of conduction electrons and local moments at low energies in the FL* phase, one therefore doesn't expect that the mutual information will be exactly zero in this phase. It vanishes only at the RG fixed point corresponding to $J_K = 0$, where these two Hilbert spaces completely decouple. In the opposite limit when the c-electrons and f-spins are maximally entangled, the Renyi mutual information will attain its maximum possible value of $4 \log(2)/5$ per site (recall that the unit cell of our model contains three f-spins and two c-electrons). In the magnetically ordered phase, one expects that the Renyi mutual information will not be close to this maximum due to the entanglement between the local moments themselves. From Fig. 3 (b) and Fig. 4 (b) we see that the QMC data is consistent with this expectation. The most notable feature is that the Renyi mutual information per site is an order of magnitude smaller in the FL* phase compared to the magnetically ordered phase. Furthermore, even on a limited size lattices such as ours, one can already see signatures of the transition from the magnetically ordered phase to the FL* phase as evidenced by the change of slope in the coefficient of the Renyi mutual information at the transition.

Conclusion and discussion: In this paper we introduced a model amenable to negative sign free Monte Carlo simulations that can host a fractionalized Fermi liquid (FL*) phase. The most prominent feature of this phase is a violation of the

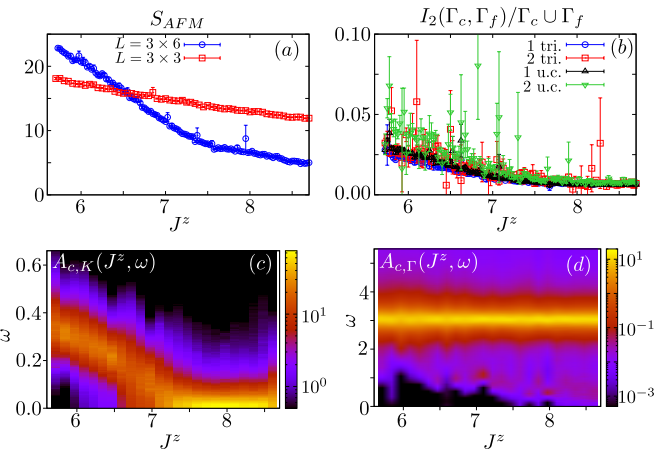


FIG. 4. (color online) We consider lattices $L = 3 \times 3$ and $L = 3 \times 6$ unit cells at an inverse temperature $\beta = 12$ and at $J_K = 1$ (a) Spin-spin correlations S_{AFM} (See text), (b) Renyi mutual informations $I_2(\Gamma_c, \Gamma_f)$ per site of the patch $\Gamma_c \cup \Gamma_f$ for $L = 3 \times 6$. Here we consider the patches listed in Fig. 2(b)-(e). (c) Conduction electron spectral function at the Dirac point \mathbf{K} for the 3×6 lattice. (d) same as (c), but at the Γ -point. The imaginary time data from which panels (c) and (d) stem are presented in the supplemental material.

Luttinger theorem due to the onset of topological order. This proof of principle calculation paves the way to many other investigations. We have considered a model where the fractionalization inherent to topological order is ‘emergent’ i.e. the lattice model is written in terms of spins. A different, and possibly numerically more tractable approach would be to simulate directly a theory of spinons coupled to \mathbb{Z}_2 gauge fields following Refs. [61–63] and where spinons are also Kondo coupled to conduction electrons. Such an approach might be particularly useful for studying the quantum phase transition between the FL* phase and the magnetically ordered phase. A field theory description of this transition was provided in Ref.[60] where it was found that the Kondo coupling is irrelevant at the critical point due to the large anomalous exponent of the spins, and therefore one expects that the conduction electrons have a well defined electron-like quasiparticle even at the critical point, while the local moments will inherit the critical exponents of the 3D XY* transition [26, 59].

It might be also interesting to explore the possibility of obtaining non-trivial symmetry protected topological phases in frustrated Kondo models along the lines of Ref. [64] where it was shown that under certain conditions, one can obtain symmetric states without any topological order even when the unit cell contains an odd number of spins but the magnetic unit cell has an integral number of spins.

Another avenue to explore would be the universal subleading contribution of the Renyi entanglement entropy for a spatial bipartition. In the FL* phase one expects that this contribution is given as $\gamma = \gamma_{\text{topo}} + \gamma_{\text{Dirac}}$, where $\gamma_{\text{topo}} = \log(2)$ is the topological entanglement entropy corresponding to the topological order of the local moments, while γ_{Dirac} is the shape-dependent universal contribution from the Dirac con-

duction electrons [65, 66]. Similarly, at the transition, owing to the aforementioned irrelevance of the Kondo coupling, one expects that $\gamma = \gamma_{\text{topo}} + \gamma_{\text{Dirac}} + \gamma_{3\text{D XY}}$ where $\gamma_{3\text{D XY}}$ is the universal shape-dependent entanglement contribution at the 3D XY transition [65].

Finally, as mentioned in the introduction, the Kondo breakdown scenario is central to several questions in heavy fermion materials as well as newly discovered frustrated Kondo lattice systems. Our approach opens a window to quantitatively explore these and related questions as well.

Acknowledgments: The authors thank T. Sato, F. Parisen-Toldin for stimulating discussions and S. Sachdev, A. Vishwanath for comments on the draft. JH and FFA are supported by the German Research Foundation (DFG), under DFG-SFB 1170 “ToCoTronics” (Project C01). TG is supported by the National Science Foundation under Grant No. DMR-1752417, and as an Alfred P. Sloan Research Fellow. The authors gratefully acknowledge the Gauss Centre for Supercomputing e.V. (www.gauss-centre.eu) for funding this project by providing computing time on the GCS Supercomputer SuperMUC at Leibniz Supercomputing Centre (LRZ, www.lrz.de). We also acknowledge the Bavaria California Technology Center (BaCaTeC) for travel support.

-
- [1] M. Imada, A. Fujimori, and Y. Tokura, *Rev. Mod. Phys.* **70**, 1039 (1998).
- [2] P. W. Anderson, *Journal of Physics C: Solid State Physics* **3**, 2436 (1970).
- [3] A. C. Hewson, *The Kondo Problem to Heavy Fermions*, Cambridge Studies in Magnetism (Cambridge University Press, Cambridge, 1997).
- [4] M. Oshikawa, *Phys. Rev. Lett.* **84**, 3370 (2000).
- [5] M. B. Hastings, *Phys. Rev. B* **69**, 104431 (2004).
- [6] E. Lieb, T. Schultz, and D. Mattis, *Annals of Physics* **16**, 407 (1961).
- [7] T. Senthil, S. Sachdev, and M. Vojta, *Phys. Rev. Lett.* **90**, 216403 (2003).
- [8] T. Senthil, M. Vojta, and S. Sachdev, *Phys. Rev. B* **69**, 035111 (2004).
- [9] J. M. Luttinger, *Phys. Rev.* **119**, 1153 (1960).
- [10] P. Coleman, C. Pépin, Q. Si, and R. Ramazashvili, *Journal of Physics: Condensed Matter* **13**, R723 (2001).
- [11] Q. Si, S. Rabello, K. Ingersent, and J. Smith, *Nature* **413**, 804 (2001).
- [12] S. Paschen, T. Lühmann, S. Wirth, P. Gegenwart, O. Trovarelli, C. Geibel, F. Steglich, P. Coleman, and Q. Si, *Nature* **432**, 881 EP (2004).
- [13] M. Klein, A. Nuber, F. Reinert, J. Kroha, O. Stockert, and H. v. Löhneysen, *Phys. Rev. Lett.* **101**, 266404 (2008).
- [14] S. Friedemann, T. Westerkamp, M. Brando, N. Oeschler, S. Wirth, P. Gegenwart, C. Krellner, C. Geibel, and F. Steglich, *Nature Phys.* **5**, 465 (2009).
- [15] M. Vojta, *J. Low Temp. Phys.* **161**, 203 (2010).
- [16] A. Dönni, G. Ehlers, H. Maletta, P. Fischer, H. Kitazawa, and M. Zolliker, *Journal of Physics: Condensed Matter* **8**, 11213 (1996).
- [17] T. Goto, S. Hane, K. Umeo, T. Takabatake, and Y. Isikawa, *Journal of Physics and Chemistry of Solids* **63**, 1159 (2002), proceedings of the 8th ISSP International Symposium.
- [18] A. Oyamada, S. Maegawa, M. Nishiyama, H. Kitazawa, and Y. Isikawa, *Physical Review B* **77**, 064432 (2008).
- [19] A. Sakai, S. Lucas, P. Gegenwart, O. Stockert, H. v. Löhneysen, and V. Fritsch, *Phys. Rev. B* **94**, 220405 (2016).
- [20] H. Oike, Y. Suzuki, H. Taniguchi, K. Miyagawa, and K. Kanoda, *ArXiv e-prints* (2016), arXiv:1602.08950 [cond-mat.str-el].
- [21] M. S. Kim, M. C. Bennett, and M. C. Aronson, *Phys. Rev. B* **77**, 144425 (2008).
- [22] K. Sengupta, M. K. Forthaus, H. Kubo, K. Katoh, K. Umeo, T. Takabatake, and M. M. Abd-Elmeguid, *Phys. Rev. B* **81**, 125129 (2010).
- [23] Y. Kato, M. Kosaka, H. Nowatari, Y. Saiga, A. Yamada, T. Kobiyama, S. Katano, K. Ohoyama, H. S. Suzuki, N. Aso, and K. Iwasa, *Journal of the Physical Society of Japan* **77**, 053701 (2008), <http://dx.doi.org/10.1143/JPSJ.77.053701>.
- [24] T. Sato, F. F. Assaad, and T. Grover, *Phys. Rev. Lett.* **120**, 107201 (2018).
- [25] L. Balents, M. P. A. Fisher, and S. M. Girvin, *Phys. Rev. B* **65**, 224412 (2002).
- [26] S. V. Isakov, Y. B. Kim, and A. Paramekanti, *Phys. Rev. Lett.* **97**, 207204 (2006).
- [27] S. V. Isakov, A. Paramekanti, and Y. B. Kim, *Phys. Rev. B* **76**, 224431 (2007).
- [28] S. V. Isakov, M. B. Hastings, and R. G. Melko, *Nat. Phys.* **7**, 772 (2011), arXiv:1102.1721 [cond-mat.str-el].
- [29] O. Derzhko, J. Richter, and M. Maksymenko, *International Journal of Modern Physics B* **29**, 1530007 (2015).
- [30] C. Honerkamp, K. Wakabayashi, and M. Sgrist, *EPL* **50**, 368 (2000), cond-mat/9902026.
- [31] A. C. Potter and P. A. Lee, *Phys. Rev. Lett.* **112**, 117002 (2014), arXiv:1303.6956.
- [32] J. S. Hofmann, F. F. Assaad, and A. P. Schnyder, *Phys. Rev. B* **93**, 201116 (2016).
- [33] E. H. Lieb, *Phys. Rev. Lett.* **62**, 1201 (1989).
- [34] M. Bercx, J. S. Hofmann, F. F. Assaad, and T. C. Lang, *Phys. Rev. B* **95**, 035108 (2017).
- [35] H. Feldner, Z. Y. Meng, T. C. Lang, F. F. Assaad, S. Wessel, and A. Honecker, *Phys. Rev. Lett.* **106**, 226401 (2011).
- [36] G. Z. Magda, X. Jin, I. Hagymási, P. Vancsó, Z. Osváth, P. Nemes-Incze, C. Hwang, L. P. Biró, and L. Tapasztó, *Nature (London)* **514**, 608 (2014).
- [37] E. Tang and L. Fu, *Nat Phys* **10**, 964 (2014).
- [38] R. Blankenbecler, D. J. Scalapino, and R. L. Sugar, *Phys. Rev. D* **24**, 2278 (1981).
- [39] S. White, D. Scalapino, R. Sugar, E. Loh, J. Gubernatis, and R. Scalettar, *Phys. Rev. B* **40**, 506 (1989).
- [40] F. Assaad and H. Evertz, in *Computational Many-Particle Physics*, Lecture Notes in Physics, Vol. 739, edited by H. Fehske, R. Schneider, and A. Weiße (Springer, Berlin Heidelberg, 2008) pp. 277–356.
- [41] F. F. Assaad, *Phys. Rev. Lett.* **83**, 796 (1999).
- [42] S. Capponi and F. F. Assaad, *Phys. Rev. B* **63**, 155114 (2001).
- [43] M. Bercx, F. Goth, J. S. Hofmann, and F. F. Assaad, *SciPost Phys.* **3**, 013 (2017), arXiv:1704.00131 [cond-mat.str-el].
- [44] A. Sandvik, *Phys. Rev. B* **57**, 10287 (1998).
- [45] K. S. D. Beach, eprint arXiv:cond-mat/0403055 (2004), cond-mat/0403055.
- [46] I. Peschel, *J. Stat. Mech.* **6**, 4 (2004), cond-mat/0403048.
- [47] T. Grover, *Phys. Rev. Lett.* **111**, 130402 (2013).
- [48] F. F. Assaad, T. C. Lang, and F. Parisen Toldin, *Phys. Rev. B* **89**, 125121 (2014), arXiv:1311.5851 [cond-mat.str-el].

- [49] J. E. Drut and W. J. Porter, Phys. Rev. B **92**, 125126 (2015), arXiv:1506.06654 [cond-mat.str-el].
- [50] J. E. Drut and W. J. Porter, Phys. Rev. E **93**, 043301 (2016), arXiv:1508.04375 [cond-mat.str-el].
- [51] F. Parisen Toldin and F. F. Assaad, ArXiv e-prints (2018), arXiv:1804.03163 [cond-mat.str-el].
- [52] P. Broecker and S. Trebst, J. Stat. Mech. **8**, 08015 (2014), arXiv:1404.3027 [cond-mat.str-el].
- [53] L. Wang and M. Troyer, Phys. Rev. Lett. **113**, 110401 (2014), arXiv:1407.0707 [cond-mat.str-el].
- [54] F. F. Assaad, Phys. Rev. B **91**, 125146 (2015), arXiv:1501.01418 [cond-mat.str-el].
- [55] P. Broecker and S. Trebst, Phys. Rev. E **94**, 063306 (2016), arXiv:1609.07309 [cond-mat.str-el].
- [56] M. B. Hastings, I. González, A. B. Kallin, and R. G. Melko, Phys. Rev. Lett. **104**, 157201 (2010), arXiv:1001.2335 [cond-mat.str-el].
- [57] S. Humeniuk and T. Roscilde, Phys. Rev. B **86**, 235116 (2012), arXiv:1203.5752 [cond-mat.str-el].
- [58] J. Becker and S. Wessel, arXiv:1803.10970 (2018), arXiv:1803.10970 [cond-mat.str-el].
- [59] A. V. Chubukov, T. Senthil, and S. Sachdev, Phys. Rev. Lett. **72**, 2089 (1994).
- [60] T. Grover and T. Senthil, Phys. Rev. B **81**, 205102 (2010).
- [61] F. F. Assaad and T. Grover, Phys. Rev. X **6**, 041049 (2016).
- [62] S. Gazit, M. Randeria, and A. Vishwanath, Nat Phys **13**, 484 (2017).
- [63] S. Gazit, F. F. Assaad, S. Sachdev, A. Vishwanath, and C. Wang, Proceedings of the National Academy of Sciences (2018), 10.1073/pnas.1806338115, <http://www.pnas.org/content/early/2018/07/06/1806338115.full.pdf>.
- [64] X. Yang, S. Jiang, A. Vishwanath, and Y. Ran, ArXiv e-prints (2017), arXiv:1705.05421 [cond-mat.str-el].
- [65] B. Swingle and T. Senthil, Phys. Rev. B **86**, 155131 (2012).
- [66] H. Yao and X.-L. Qi, Phys. Rev. Lett. **105**, 080501 (2010).

| U | σ^x | σ^z | σ^0 | σ^0 |
|-----------|------------|------------|------------|------------|
| α | - | - | + | - |
| β_x | - | + | - | - |
| β_y | + | + | + | - |
| β_z | + | - | - | - |

TABLE I. Table of independent particle-hole symmetries. See the supplemental material text for the notation.

Supplemental Material for

“Kondo Breakdown via Fractionalization in a Frustrated Kondo Lattice Model”

Authors: Johannes S. Hofmann, Fakher F. Assaad and Tarun Grover

I. SYMMETRIES AND HEAVY FERMION LIQUIDS

Our model, Eq.(1), has several continuous and discrete symmetries. Among continuous symmetries, the number of conduction electrons is conserved, and so is the projection of the total spin along the z-direction, i.e., $\sum_{\mathbf{x}} \hat{S}_{\mathbf{x}}^{c,z} + \sum_{\mathbf{i}} \hat{S}_{\mathbf{i}}^{f,z}$.

The model also exhibits several unitary and anti-unitary particle-hole symmetries which we list in Table I. They are implemented by a matrix U via $\hat{c}_{\mathbf{x},s}^\dagger \rightarrow (-1)^{\mathbf{x}} U_{s,s'} \hat{c}_{\mathbf{x},s'}$ and $\hat{f}_{\mathbf{i},s}^\dagger \rightarrow U_{s,s'} \hat{f}_{\mathbf{i},s'}$ together with the sign α distinguishing between unitary and anti-unitary transformations: $\sqrt{-1} \rightarrow \alpha\sqrt{-1}$. We list their action on the spin operators by the signs $\boldsymbol{\beta} = (\beta_x, \beta_y, \beta_z)$ with $\hat{S}_{\mathbf{x}}^{c,l} \rightarrow \beta_l \hat{S}_{\mathbf{x}}^{c,l}$ as well as $\hat{S}_{\mathbf{i}}^{f,l} \rightarrow \beta_l \hat{S}_{\mathbf{i}}^{c,l}$.

One can also combine the particle-hole symmetries in Table I to define two different anti-unitary time-reversal symmetries. The first one, TR_1 , is defined via $\hat{c}_{\mathbf{x},s}^\dagger \rightarrow i\sigma_{s,s'}^y \hat{c}_{\mathbf{x},s'}$ and $\hat{f}_{\mathbf{i},s}^\dagger \rightarrow i\sigma_{s,s'}^y \hat{f}_{\mathbf{i},s'}$ along with $\sqrt{-1} \rightarrow -\sqrt{-1}$. This transformation flips all three components of the spin operators $\hat{S}_{\mathbf{x}}^c \rightarrow -\hat{S}_{\mathbf{x}}^c$ as well as $\hat{S}_{\mathbf{i}}^f \rightarrow -\hat{S}_{\mathbf{i}}^f$. The second one, TR_2 , replaces $i\sigma^y$ by σ^x so that only the z-component of the spin operators gets reversed.

At the level of free fermion band-structure, the particle-hole symmetries listed above lead to flat bands. In particular, either of the symmetries $(U, \alpha) = (\sigma^0, -)$ and $(U, \alpha) = (\sigma^z, -)$ guarantee that there is a flat band. This is because these transformations do not mix up and down spin components, which leads to an odd number (=five) of bands for each spin sector. Furthermore, the anti-unitary nature of the symmetry implies that $c(k) \rightarrow c^\dagger(k)$. Thus there always exists a flat band at zero energy in each spin sector. Such a flat band will generically be unstable to interactions, e.g., according to Table I, a magnetically ordered state in the z-direction will break both of these particle-hole symmetries.

Let us next consider heavy fermion phases that result from the hybridization of c- and f-electrons. As just discussed,

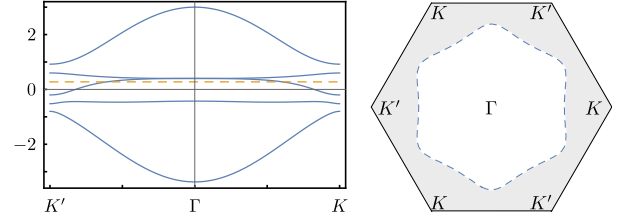


FIG. 5. (color online) Cut of the spectrum from K' to K with the Fermi energy marked by the dashed, orange line constraint to the half filled case and Fermi surface (blue, dashed) of a heavy Fermi Liquid state with $\Delta = 0.4$ and $t' = 0.2$. The shaded area marks the occupied part of the BZ.

to obtain dispersive bands one would need to break at least some symmetries. One option is a uniform hybridization, $\sum_{\langle \mathbf{x}, \mathbf{i} \rangle, s} \hat{c}_{\mathbf{x},s}^\dagger \hat{f}_{\mathbf{i},s} + h.c.$, that preserves the time reversal symmetries TR_1 and TR_2 , but breaks all the particle-hole symmetries. As a consequence, one should also allow direct f-electron hopping terms given by $\sum_{\langle \mathbf{i}, \mathbf{j} \rangle, s} \hat{f}_{\mathbf{i},s}^\dagger \hat{f}_{\mathbf{j},s} + h.c.$. The mean-field Hamiltonian for such a heavy Fermi Liquid is then given as

$$\hat{H}_{\text{hFL}} = \hat{H}_c + \Delta \sum_{\langle \mathbf{x}, \mathbf{i} \rangle, s} \hat{c}_{\mathbf{x},s}^\dagger \hat{f}_{\mathbf{i},s} + t' \sum_{\langle \mathbf{i}, \mathbf{j} \rangle, s} \hat{f}_{\mathbf{i},s}^\dagger \hat{f}_{\mathbf{j},s} + h.c. \quad (2)$$

The resulting band-structure is depicted in Fig. 5 for $\Delta = 0.4$ and $t' = 0.2$, where the left hand side shows a cut from K' to Γ to K . We clearly recognize a dispersive band in the middle of the spectrum replacing the aforementioned flat band at zero energy. Each band is spin degenerate which enhances the S_z symmetry to a full $SU(2)$ and consequently, the state is paramagnetic. The right hand side of the figure shows the Fermi surface (blue, dashed) where we have kept the electron density fixed at the half-filling. Consistent with the Oshikawa's argument [4], one finds that the Fermi surface is ‘large’, and occupies half of the Brillouin zone which is depicted by the shaded area in Fig.5. The effective chemical potential required for the half filling is marked by the dashed orange line in the middle panel.

Finally, one may also consider hybridization of the form $\sum_{\langle \mathbf{x}, \mathbf{i} \rangle} \hat{c}_{\mathbf{x},\uparrow}^\dagger \hat{f}_{\mathbf{i},\uparrow} - (-1)^{\mathbf{x}} \hat{c}_{\mathbf{x},\downarrow}^\dagger \hat{f}_{\mathbf{i},\downarrow} + h.c.$ which preserves the particle-hole symmetry listed as $(\sigma^x, -)$ in Table I, but still breaks $(\sigma^z, -)$, $(\sigma^0, +)$ and $(\sigma^0, -)$, as well as TR_1 and TR_2 . This mean-field is also motivated by the structure of our Hamiltonian where the Kondo interaction has an additional sign that depends on the sublattice. Due to time-reversal symmetry breaking, such a state will generically result in magnetization along the z-direction.

II. DETAILS ON THE METHOD

Let us first write down the fermionized Hamiltonian that is simulated, \hat{H}_{qmc} , and then show its equivalence to Eq. (1).

$$\hat{H}_{\text{qmc}} = -t \sum_{\langle \mathbf{x}, \mathbf{y} \rangle, \sigma} \hat{c}_{\mathbf{x}, \sigma}^\dagger \hat{c}_{\mathbf{y}, \sigma} + h.c. - \frac{J^\perp}{4} \sum_{\langle \mathbf{i}, \mathbf{j} \rangle} \left[2 \left(\sum_{\sigma} \hat{f}_{\mathbf{i}, \sigma}^\dagger \hat{f}_{\mathbf{i}, \sigma} + h.c. \right)^2 + \left(n_{\mathbf{i}}^f + n_{\mathbf{j}}^f - 1 \right)^2 \right] - \frac{J^z}{4} \sum_{\square} \sum_{\mathbf{i}_\square < \mathbf{j}_\square} \left(n_{\mathbf{i}}^f - n_{\mathbf{j}}^f \right)^2 - \frac{J_K}{4} \sum_{\langle \mathbf{i}, \mathbf{x} \rangle} \left(\sum_{\sigma} \hat{f}_{\mathbf{i}, \sigma}^\dagger \hat{c}_{\mathbf{x}, \sigma} + h.c. \right)^2, \quad (3)$$

with $(\hat{c}_{\mathbf{x}, \uparrow}^\dagger, \hat{c}_{\mathbf{x}, \downarrow}^\dagger) = (\hat{c}_{\mathbf{x}, \uparrow}^\dagger, (-1)^{\mathbf{x}} \hat{c}_{\mathbf{x}, \downarrow}^\dagger)$ and $(\hat{f}_{\mathbf{i}, \uparrow}^\dagger, \hat{f}_{\mathbf{i}, \downarrow}^\dagger) = (\hat{f}_{\mathbf{i}, \uparrow}^\dagger, \hat{f}_{\mathbf{i}, \downarrow}^\dagger)$. The Hamiltonian above is identical to Eq. (1) up to the following five terms in $\hat{H}_{\text{qmc}} - \hat{H}$. The first term $+(J^\perp + 4J^z) \sum_{\mathbf{i}} (n_{\mathbf{i}}^f - 1)^2$ is the well known repulsive Hubbard interaction that suppress charge fluctuations. The local parity of the f -electrons $(n_{\mathbf{i}}^f - 1)^2$ commutes with the Hamiltonian as the relevant terms $+J^\perp \sum_{\langle \mathbf{i}, \mathbf{j} \rangle} \hat{f}_{\mathbf{i}, \uparrow}^\dagger \hat{f}_{\mathbf{i}, \downarrow}^\dagger \hat{f}_{\mathbf{j}, \downarrow} \hat{f}_{\mathbf{j}, \uparrow} + h.c.$ and $+\frac{J_K}{2} \sum_{\langle \mathbf{i}, \mathbf{x} \rangle} (-1)^{\mathbf{x}} \hat{f}_{\mathbf{i}, \uparrow}^\dagger \hat{f}_{\mathbf{i}, \downarrow}^\dagger \hat{c}_{\mathbf{x}, \downarrow} \hat{c}_{\mathbf{x}, \uparrow} + h.c.$ modify the local occupation by 2. Hence the Hubbard interaction projects onto the sector with singly occupied f -electron sites exponentially fast and the relevant scale is set by $\beta(J^\perp + 4J^z)$. In this subspace, all other contributions of $+\frac{J^\perp}{2} \sum_{\langle \mathbf{i}, \mathbf{j} \rangle} (n_{\mathbf{i}}^f - 1)(n_{\mathbf{j}}^f - 1)$ and $+\frac{J_K}{4} \sum_{\langle \mathbf{i}, \mathbf{x} \rangle} (n_{\mathbf{i}}^f - 1)(n_{\mathbf{x}}^c - 1)$, vanish such that $\hat{H}_{\text{qmc}}|_{(n_{\mathbf{i}}^f - 1)^2=0} = \hat{H}$. The interested reader is referred to the supplemental material, i.e. Eq. (9), of Ref. [24].

The efficient projection due to the repulsive Hubbard interaction however also introduces a challenge for the numerical stability of the algorithm. Here we have to control the various scales of $A_j = \prod_{i=0}^j B_i$ where B_i is the product of all exponentiated operators on the i th time slice. Apparently, this model generated Eigenvalues in A_j which exceeded the range of double precision which is of order $10^{\pm 308}$. To overcome this issue, we implemented the following stabilization scheme. Assume that we already have a QR decomposition of $A_{j-1} = Q_{j-1} e^{\lambda_{j-1}} R_{j-1}$ where Q_{j-1} is the orthogonal part, $e^{\lambda_{j-1}}$ is diagonal and separates the main scales, and R_{j-1} contains the mixing of them. To generate $A_j = B_j A_{j-1}$ we perform the following steps:

1. Calculate $M_j = B_j Q_{j-1}$
2. Use the permutation P_j to sort the columns of $M_j = \tilde{M}_j P_j$ according to the column norm of $M_j e^{\lambda_{j-1}}$. Permute λ_{j-1} and R_{j-1} with P_j^{-1} to correct this manipulation
3. Perform a QR decomposition of $M_j = Q_j \tilde{R}_j$ without pivoting.
4. Extract the scales of \tilde{R} as $(D_j)_n = |(\tilde{R}_j)_{nn}|$.
5. Determine the new scales $\lambda_j = \log(D_j) + \lambda_{j-1}$.
6. Calculate $R_j = D_j^{-1} e^{-\lambda_{j-1}} \tilde{R}_j e^{\lambda_{j-1}} R_{j-1}$

This scheme keeps all the advantages of QR decomposition with pivoting to handle exponentially large and small scales of

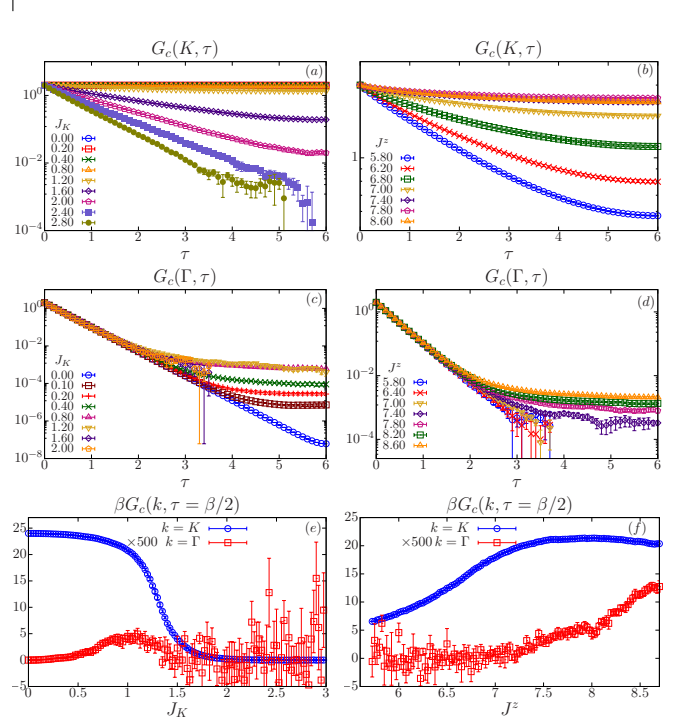


FIG. 6. (color online) The simulations were performed on the $L = 3 \times 6$ lattice at an inverse temperature of $\beta = 12$. Left panels corresponds to the J_K scan at $J^z = 7.5$ and the right to the J^z scan at $J_K = 1.0$. For large J_K or small J^z , we restricted the time domain in (c) and (d) to $\tau < 3.5$ and $\tau < 3.75$, respectively, since beyond this scale, the data becomes very noisy.

A_j which is paramount to a stable BSS algorithm, even when double precision suffices. Here, we did not store the scales as D 's but rather as $e^{\lambda_{j-1}}$ to handle numbers much larger than $10^{\pm 308}$.

III. TIME DISPLACED GREENS FUNCTION

Here we provide the imaginary time displaced Greens functions of conduction electrons, $G_c(\mathbf{k}, \tau) = \sum_{\alpha, \sigma} \langle \hat{c}_{\mathbf{k}, \alpha, \sigma}^\dagger(\tau) \hat{c}_{\mathbf{k}, \alpha, \sigma}(0) \rangle$ where α is the orbital and σ the spin index. The dynamical data presented in the main text, is obtained by solving

$$G_c(\mathbf{k}, \tau) = \frac{1}{\pi} \int d\omega \frac{e^{-\tau\omega}}{1 + e^{-\beta\omega}} A_c(\mathbf{k}, \omega) \quad (4)$$

for $A_c(\mathbf{k}, \omega)$ using the stochastic maximum entropy method [44, 45]. The features present in the dynamical data can

clearly be detected in the imaginary time data which we report in this section. In Fig. 6, the left hand side panels presents the J_K scan at a fixed $J^z = 7.5$ whereas on the right hand side we show the J^z scan at constant $J_K = 1.0$.

Panels (a) and (b) depicts the Greens function at the Dirac points. In both cases, the gapless mode is clearly visible in the FL* phase since $G_c(\mathbf{K}, \tau)$ shows a plateau at *large* imaginary times. This height of the plateau corresponds to the quasi-particle residue.

Panels (c) and (d) present the equivalent data but at the Γ point. In the FL* phase we see a clear feature with small intensity at *large* values of τ . It is this feature in the imaginary time Green function that generates the low energy spectral weight in Fig. 3(d) and Fig. 4(d) in the FL* phase. As mentioned in the article, we interpret this feature as a signature of the vison excitation.

Another possible analysis stems from the identity,

$$\lim_{\beta \rightarrow \infty} \beta G_c(\mathbf{k}, \tau = \beta/2) = A_c(\mathbf{k}, \omega = 0), \quad (5)$$

that holds provided that $A_c(\mathbf{k}, \omega)$ is a smooth function. At finite values of β , $\beta G_c(\mathbf{k}, \tau = \beta/2)$ will provide an estimate of the spectral weight in an energy window around $\omega = 0$ of width set by $1/\beta$. Panels (e) and (f) plot this quantity both at the Γ and Dirac points. Overall, these panels again confirm that in the FL* phase we observe low energy excitations with small intensity at the Γ point and low energy excitations with large spectral weight at the Dirac point. Note that in panel (e), corresponding to the J_K scan, the intensity of the feature at the Γ point first grows and then decreases since both at $J_K = 0$, where the spin and conduction electrons decouple and the conduction electrons form a Dirac spectrum, and at $J_K \gg 1$ where in the magnetic insulating phase, no low lying single particle weight is expected at the Γ point.